Nano Research
2021, 14(6): 1659–1662
ISSN 1998-0124 CN 11-5974/O4
https://doi.org/10.1007/s12274-020-2859-9

Research Article

Fast growth of large single-crystalline WS_2 monolayers via chemical vapor deposition

Shengxue Zhou[1,2], Lina Liu[1], Shuang Cui[3], Xiaofan Ping[1], Dake Hu[1], and Liying Jiao[1] (✉)

[1] *Key Laboratory of Organic Optoelectronics and Molecular Engineering of the Ministry of Education, Department of Chemistry, Tsinghua University, Beijing 100084, China*
[2] *Department of Chemistry and Chemical Engineering, Ningxia Normal University, Guyuan 756000, China*
[3] *Sinopec Beijing Research Institute of Chemical Industry, Beijing 100013, China*

Received: 3 March 2020 / **Revised:** 3 May 2020 / **Accepted:** 8 May 2020

ABSTRACT

Two-dimensional (2D) tungsten disulfide (WS_2) has emerged as a promising ultrathin semiconductor for building high-performance nanoelectronic devices. The controllable synthesis of WS_2 monolayers (1L) with both large size and high quality remains as a challenge. Here, we developed a new approach for the chemical vapor deposition (CVD) growth of WS_2 monolayers by using K_2WS_4 as the growth precursor. The simple chemistry involved in our approach allowed for improved controllability and a fast growth rate of ~ 30 μm·min^{-1}. We achieved the reliable growth of 1L WS_2 flakes with side lengths of up to ~ 500 μm and the obtained WS_2 flakes were 2D single crystals with low density of defects over a large area as evidenced by various spectroscopic and microscopic characterizations. In addition, the large 1L WS_2 single crystals we obtained showed higher electrical performance than their counterparts grown with previous approaches, demonstrating the potential of our approach in producing high quality and large 2D semiconductors for future nanoelectronics.

KEYWORDS

tungsten disulfide, two-dimensional, chemical vapor deposition, field effect transistors

1 Introduction

Two-dimensional (2D) semiconducting transition metal dichalcogenides (TMDCs) provides ultra-thin channel materials for constructing ultra-short channel field effect transistors (FETs). Single-layered (1L) WS_2 is a typical 2D semiconductor with a direct bandgap of 2.05 eV [1–3] and has shown promising applications in FETs [4, 5], photodetectors [6–8], and electrocatalysis [9, 10]. To promote the practical applications of 2D WS_2 in electronics and optoelectronics, it is essential to realize the controlled synthesis of high quality 1L WS_2 with large size, ideally in the form of single crystalline monolayers. Currently, 1L WS_2 single crystalline flakes can be obtained by using WO_x and sulfur as the growth precursors via chemical vapor deposition (CVD). However, the reactions involved in the sulfurization of WO_x are complicated and the detailed mechanism has not been fully understood [11], in addition, it is difficult to maintain the molar ratio between WO_x and S in the gas phase throughout the growth process [12, 13]. As a result, the density of defects in the obtained WS_2 flakes may increase as the growth proceeds and consequently, leading to the degradation of crystal quality [14, 15] and electrical performance [16, 17] in larger WS_2 flakes. The mobility of smaller WS_2 monolayers with a side length of tens of micrometers can be up to ~ 50 cm^2·V^{-1}·s^{-1}, however, the mobility dropped to < 2 cm^2·V^{-1}·s^{-1} for samples with side lengths of > 450 μm [18, 19]. Therefore, it is highly desirable to develop controllable approach for synthesizing single crystalline WS_2 monolayers with both large size and high electrical quality.

In this work, we present a controllable approach for the CVD growth of single crystalline 1L WS_2 by using K_2WS_4 as the growth precursor. The chemistry involved in the formation of WS_2 is simply the thermal decomposition reaction of K_2WS_4 and therefore, allows for improved controllability for the growth of WS_2 than using WO_x and S as precursors. In addition, with this approach, the growth rate of WS_2 monolayers can reach up to ~ 30 μm·min^{-1}, which is the fastest rate reported so far in the growth of 2D single crystalline WS_2. We obtained triangular 1L WS_2 flakes with side lengths of up to ~ 500 μm and averaged mobility of ~ 10 cm^2·V^{-1}·s^{-1}, which is obviously higher than 1L WS_2 flakes with similar size obtained by other approaches. Our work opens a new way for the controllable growth of large 2D TMDCs with high quality for the practical applications of these ultrathin semiconductors in electronic devices.

Our approach for the growth of large single crystalline WS_2 monolayers is simply based on the thermal decomposition of K_2WS_4 as shown in the following reaction equation

$$K_2WS_4 \xrightarrow{860\,^{\circ}C} WS_2 + K_2S + S \quad (1)$$

K_2WS_4 precursors were synthesized following the procedures described in the Electronic Supplementary Material (ESM) (Fig. S1 in the ESM). The obtained precursors were loaded on a freshly-cleaved fluorophlogopite mica substrate and then the substrate was placed in the center of a horizonal CVD furnace. The growth was carried out under atmospheric pressure using Ar/H_2 as the carrier gas as schematically shown in Fig. 1(a).

Address correspondence to lyjiao@tsinghua.edu.cn

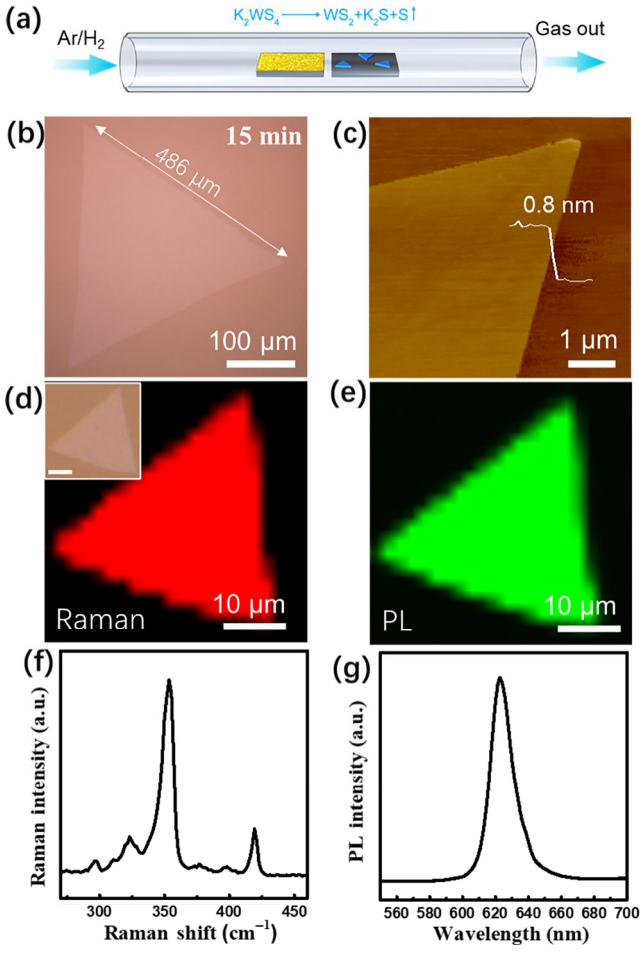

Figure 1 Growth of WS_2 monolayers with K_2WS_4. (a) Schematics for the CVD growth of large-area single crystalline WS_2 monolayers. (b) Optical image of a typical WS_2 triangular flake grown on mica. (c) AFM image of a corner of a typical WS_2 flake with a height of ~ 0.8 nm. (d)–(g) Raman and PL mapping images and spectra of the WS_2 flake shown in the inset of (d), respectively. Scale bar in the inset of (d): 10 μm.

Individual WS_2 triangular flakes with side lengths of up to ~ 500 μm were obtained on mica substrates over a large area after the CVD growth of 15 min at 860 °C (Fig. 1(b)), and prolonged growth (> 20 min) resulted in a continuous film with length of centimeters (Fig. 3(c)). The thickness of the obtained flakes measured with atomic force microscopy (AFM) was ~ 0.8 nm (Fig. 1(c)), indicating the monolayer nature of the as-grown WS_2 flakes [21, 22]. Raman and photoluminescence (PL) spectroscopy were employed to characterize the as-grown WS_2 flakes. Two characteristic Raman peaks at ~ 350 and ~ 417 cm^{-1} were observed on WS_2 flakes which can be assigned to E^1_{2g} and A_{1g} modes of WS_2, respectively (Fig. 1(f)). And a strong PL peak located at ~ 623 nm was observed on the obtained flakes (Fig. 1(g)), further indicating that the flakes were monolayers [23, 24]. Raman and PL mapping images collected on a typical WS_2 flake displayed almost identical intensities over the whole flake (Figs. 1(d) and 1(e)), demonstrating high spatial uniformity of the as-grown WS_2 samples. The binding energies for both W and S elements measured on the obtained samples with X-ray photoelectron spectroscopy (XPS) (Fig. S3 in the ESM) were consistent with the values of WS_2 in 2H phase [2, 5, 22, 24, 25] and the atomic ratio of W:S was estimated to be 1:2, further suggesting the high purity of the obtained WS_2 [26, 27].

To investigate the crystallinity and atomic structure of the obtained WS_2 flakes, we imaged the obtained samples with transmission electron microscopy (TEM) and scanning transmission electron microscopy (STEM) by transferring the as-grown WS_2 samples to holey carbon TEM grids via water-assisted peeling (Fig. S4 in the ESM) [28]. Selected-area electron diffraction (SAED) patterns acquired at multiple positions of a WS_2 flake with a side length of ~ 400 μm (Fig. 2(a)) showed identical sets of hexagonal symmetrical spots (Figs. 2(b) and 2(c), and Figs. S5(e)–S5(h) in the ESM). The averaged orientation angle (θ) of six-symmetrical hexagonal spots of the SAED patterns collected at varied positions was 65.3° ± 0.2° (Fig. 2(d)), demonstrating the single crystalline nature of the obtained WS_2 monolayers over the whole flake. Atomically-resolved STEM images taken at multiple locations on the basal plane of the

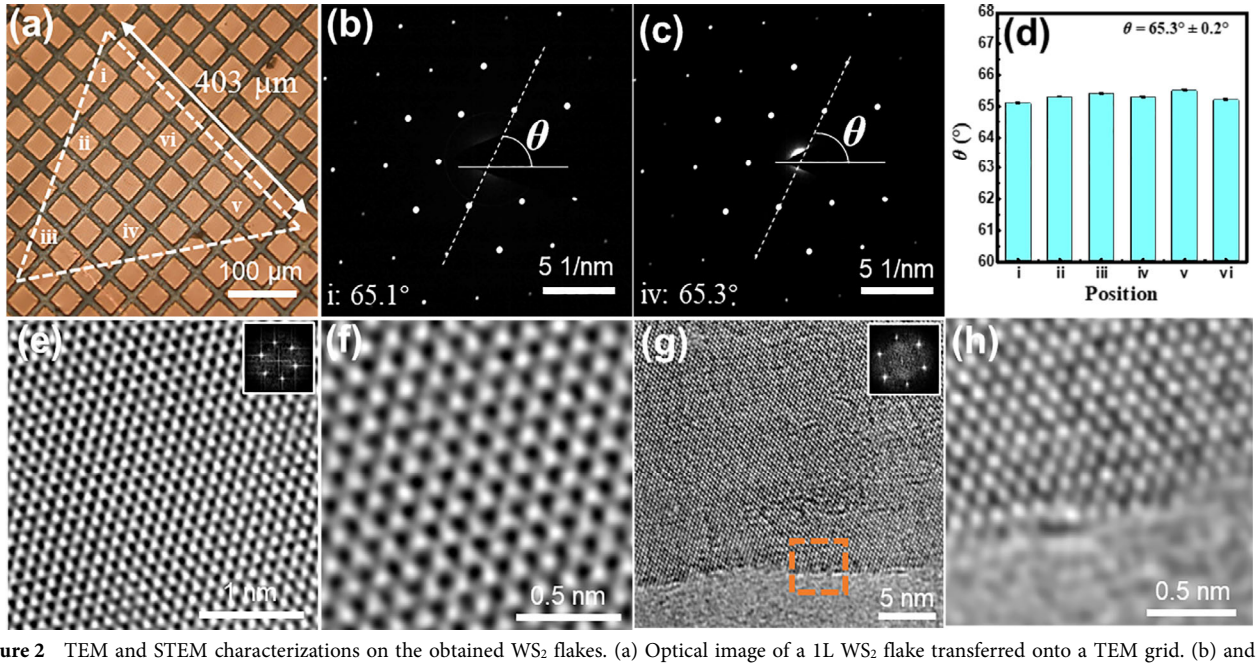

Figure 2 TEM and STEM characterizations on the obtained WS_2 flakes. (a) Optical image of a 1L WS_2 flake transferred onto a TEM grid. (b) and (c) SAED patterns collected at positions marked with i and iv on the same flake shown in (a) (see SAED patterns of more positions in Fig. S5 in the ESM). (d) Histogram of the orientation angles of hexagonal spots in SAED patterns collected at different positions on the flake shown in (a). (e) and (f) STEM images taken from the basal plane of a 1L flake, showing no observable defects. (g) and (h) STEM images taken at the edge of a 1L WS_2 flake, showing W terminated zig-zag edge. The insets of (e) and (g) are corresponding FFT patterns.

WS_2 flakes exhibited orderly arranged hexagonal packing of W and S atoms without observable defects (Fig. 2(e) and 2(f), and Figs. S5(b)–S5(d) in the ESM), further demonstrating the high quality of our WS_2 monolayers over a large area. The STEM images captured at the edges of the obtained WS_2 flake displayed W-terminated zig-zag edge structures [29] (Figs. 2(g) and 2(h)).

We attributed the successful growth of large single crystalline WS_2 monolayers to both the constant supply of WS_2 in the gas phase and the fast growth rate by using K_2WS_4 as the growth precursor. To estimate the growth rate of WS_2 with our approach, we captured the optical images of WS_2 grown on mica substrates after varied growth duration (Figs. 3(a)–3(c) and 1(b)) and observed that the side lengths of the obtained flakes increased from 60 to ~ 500 μm by tuning the growth time from 5 to 15 min and growth rate was estimated to be ~ 30 μm·min^{-1} (Fig. 3(d) and Fig. S2 in the ESM), which was obviously faster than the previously reported growth rates (0.2–20 μm·min^{-1}) for the CVD growth of WS_2 on insulating substrates [30].

The high quality and large size of our WS_2 flakes made them ideal channel materials for constructing high performance FETs. To evaluate the electrical performance of the as-grown WS_2 flakes, we fabricated back-gated FETs on SiO_2/Si substrates with transferred WS_2 flakes by electron beam lithography (EBL) and thermal deposition of 10 nm Cr/100 nm Au as source and drain electrodes. The devices were measured at room temperature in vacuum (~ 10^{-5} mbar). The transfer characteristics of a typical 1L WS_2 flake exhibited intrinsic n-type conduction with an on/off current ratio of ~ 5.5×10^8 (Figs. 4(a) and 4(b)). The field effect mobility of this device was estimated to be ~ 13.8 cm^2·V^{-1}·s^{-1}. It is worth noting that the total 20 FETs we fabricated all showed on/off current ratios in the range of 1.6×10^7–5.5×10^8 and mobilities of 4–14 cm^2·V^{-1}·s^{-1} (Fig. 4(c)). Compared with previously reported results, the electrical performance of our WS_2 samples was superior to 1L WS_2 flakes larger than 300 μm grown with other approaches (Fig. S6 in the ESM) [18, 19, 31]. To further evaluate the uniformity of the as-grown monolayer WS_2, we fabricated FETs with multiple channels on a strip of our WS_2 flake patterned by EBL and plasma etching (Fig. 4(d)). We measured the contact resistance (R_c) and the FET properties using the transmission line method (TLM) [32] and extracted a R_c of 7.7 kΩ·μm which was ~ 4 times lower than that of ~ 35 kΩ·μm reported in the literature also with Cr/Au as electrodes [33, 34]. And the mobilities were almost unchanged as the channel lengths varied (Fig. 4(d)), demonstrating the potential of our samples in fabricating large arrays of devices with identical performances.

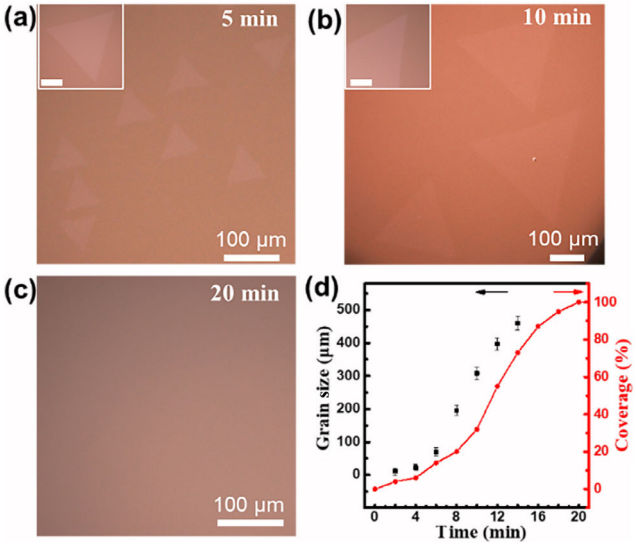

Figure 3 Optical images of as-grown 1L WS_2 flakes obtained after a growth duration of (a) 5 min, (b) 10 min, and (c) 20 min, respectively. (d) The flake size and coverage of the obtained WS_2 flakes as a function of the growth time. The insets in (a) and (b) are corresponding zoomed-in images, scale bar: 20 μm.

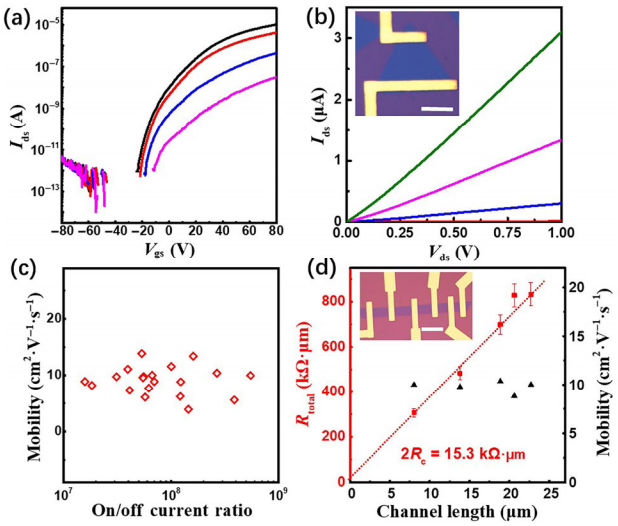

Figure 4 Electrical performances of the obtained WS_2 monolayer. (a) I_{ds}–V_{gs} curves of a device fabricated with a typical 1L WS_2 flake (inset of (b)), measured at various bias voltages of 1 V, 500 mV, 100 mV and 10 mV, respectively, from top to bottom. (b) I_{ds}–V_{ds} output characteristics for the same device under various gate voltages from 80 to 0 V at a step of 20 V from top to bottom, respectively. (c) Distributions of the estimated mobility and on/off current ratio of 20 FETs fabricated on 1L WS_2 flakes. (d) Resistances and mobilities of FETs with varied channel length fabricated on a strip of 1L WS_2 flake. Inset (b) and (d): the optical images of the measured devices in (a) and (d), respectively, scale bar: 20 μm.

In summary, we reported the successful growth of large-size single-crystalline WS_2 monolayers by using K_2WS_4 as precursor. The direct production of WS_2 by the thermal decomposition of K_2WS_4 in the gas phase allows for faster and more controllable growth of WS_2 monolayers in comparison with using other growth precursors, such as WO_x and S. With this approach, we obtained single crystalline 1L WS_2 flakes with side length of up to ~ 500 μm and averaged mobility of ~ 10 cm^2·V^{-1}·s^{-1}, which is superior to samples with similar size grown with other approaches. Our work elucidates the importance of the growth precursors in the growth of 2D TMDCs and also makes high quality 1L WS_2 easily accessible for constructing high performance electronic devices.

Acknowledgements

We acknowledge the National Natural Science Foundation of China (Nos. 21875127 and 21925504) and Tsinghua University Initiative Scientific Research Program.

Electronic Supplementary Material: Supplementary material (for more information on further details of the synthesis of K_2WS_4 precursor; the growth, characterizations, and transfer of the obtained 1L WS_2 flakes; the estimation of the growth rate; device fabrication and measurement, and more data on the obtained 1L WS_2 flakes) is available in the online version of this article at https://doi.org/10.1007/s12274-020-2859-9.

References

[1] Ye, Z. L.; Cao, T.; O'Brien, K.; Zhu, H. Y.; Yin, X. B.; Wang, Y.; Louie, S. G.; Zhang, X. Probing excitonic dark states in single-layer tungsten disulphide. *Nature* **2014**, *513*, 214–218.

[2] Mak, K. F.; Shan, J. Photonics and optoelectronics of 2D semiconductor transition metal dichalcogenides. *Nat. Photonics* **2016**, *10*, 216–226.

[3] Wang, Y. L.; Cong, C. X.; Yang, W. H.; Shang, J. Z.; Peimyoo, N.; Chen, Y.; Kang, J. Y.; Wang, J. P.; Huang, W.; Yu, T. Strain-induced direct–indirect bandgap transition and phonon modulation in monolayer WS_2. *Nano Res*. **2015**, *8*, 2562–2572.

[4] Cui, Y.; Xin, R.; Yu, Z. H.; Pan, Y. M.; Ong, Z. Y.; Wei, X. X.; Wang, J. Z.; Nan, H. Y.; Ni, Z. H.; Wu, Y. et al. High-performance monolayer WS_2 field-effect transistors on high-κ dielectrics. *Adv. Mater*. **2015**, *27*, 5230–5234.

[5] Zhang, F.; Lu, Y. F.; Schulman, D. S.; Zhang, T. Y.; Fujisawa, K.; Lin, Z.; Lei, Y.; Elias, A. L.; Das, S.; Sinnott, S. B. et al. Carbon doping of WS_2 monolayers: Bandgap reduction and p-type doping transport. *Sci. Adv*. **2019**, *5*, eaav5003.

[6] Mehew, J. D.; Unal, S.; Alonso, E. T.; Jones, G. F.; Ramadhan, S. F.; Craciun, M. F.; Russo, S. Fast and highly sensitive ionic-polymer-gated WS_2-graphene photodetectors. *Adv. Mater*. **2017**, *29*, 1700222 .

[7] Yeh, C. H.; Chen, H. C.; Lin, H. C.; Lin, Y. C.; Liang, Z. Y.; Chou, M. Y.; Suenaga, K.; Chiu, P. W. Ultrafast monolayer In/Gr-WS_2-Gr hybrid photodetectors with high gain. *ACS Nano* **2019**, *13*, 3269–3279.

[8] Kim, B. H.; Gu, H. H.; Yoon, Y. J. Large-area and low-temperature synthesis of few-layered WS_2 films for photodetectors. *2D Mater*. **2018**, *5*, 045030.

[9] Choi, C. L.; Feng, J.; Li, Y. G.; Wu, J.; Zak, A.; Tenne, R.; Dai, H. J. WS_2 nanoflakes from nanotubes for electrocatalysis. *Nano Res*. **2013**, *6*, 921–928.

[10] Zhang, Y. S.; Shi, J. P.; Han, G. F.; Li, M. J.; Ji, Q. Q.; Ma, D. L.; Zhang, Y.; Li, C.; Lang, X. Y.; Zhang, Y. F. et al. Chemical vapor deposition of monolayer WS_2 nanosheets on Au foils toward direct application in hydrogen evolution. *Nano Res*. **2015**, *8*, 2881–2890.

[11] Zhang, Y.; Yao, Y. Y.; Sendeku, M. G.; Yin, L.; Zhan, X. Y.; Wang, F.; Wang, Z. X.; He, J. Recent progress in CVD growth of 2D transition metal dichalcogenides and related heterostructures. *Adv. Mater.* **2019**, *31*, 1901694.

[12] Thangaraja, A.; Shinde, S. M.; Kalita, G.; Tanemura, M. Effect of WO_3 precursor and sulfurization process on WS_2 crystals growth by atmospheric pressure CVD. *Mater. Lett*. **2015**, *156*, 156–160.

[13] Cho, D. H.; Lee, W. J.; Wi, J. H.; Han, W. S.; Yun, S. J.; Shin, B.; Chung, Y. D. Enhanced sulfurization reaction of molybdenum using a thermal cracker for forming two-dimensional MoS_2 layers. *Phys. Chem. Chem. Phys*. **2018**, *20*, 16193–16201.

[14] Kastl, C.; Koch, R. J.; Chen, C. T.; Eichhorn, J.; Ulstrup, S.; Bostwick, A.; Jozwiak, C.; Kuykendall, T. R.; Borys, N. J.; Toma, F. M. et al. Effects of defects on band structure and excitons in WS_2 revealed by nanoscale photoemission spectroscopy. *ACS Nano* **2019**, *13*, 1284–1291.

[15] Lin, Y. C.; Li, S. S.; Komsa, H. P.; Chang, L. J.; Krasheninnikov, A. V.; Eda, G. K.; Suenaga, K. Revealing the atomic defects of WS_2 governing its distinct optical emissions. *Adv. Funct. Mater*. **2018**, *28*, 1704210.

[16] Qiu, H.; Xu, T.; Wang, Z. L.; Ren, W.; Nan, H. Y.; Ni, Z. H.; Chen, Q.; Yuan, S. J.; Miao, F.; Song, F. Q. et al. Hopping transport through defect-induced localized states in molybdenum disulphide. *Nat. Commun*. **2013**, *4*, 2642.

[17] Schuler, B.; Lee, J. H.; Kastl, C.; Cochrane, K. A.; Chen, C. T.; Refaely-Abramson, S.; Yuan, S. J.; van Veen, E.; Roldán, R.; Borys, N. J. et al. How substitutional point defects in two-dimensional WS_2 induce charge localization, spin-orbit splitting, and strain. *ACS Nano* **2019**, *13*, 10520–10534.

[18] Lan, C. Y.; Kang, X. L.; Wei, R. J.; Meng, Y.; Yip, S. P.; Zhang, H.; Ho, J. C. Utilizing a NaOH promoter to achieve large single-domain monolayer WS_2 films via modified chemical vapor deposition. *ACS Appl. Mater. Interfaces* **2019**, *11*, 35238–35246.

[19] Gao, Y.; Liu, Z. B.; Sun, D. M.; Huang, L.; Ma, L. P.; Yin, L. C.; Ma, T.; Zhang, Z. Y.; Ma, X. L.; Peng, L. M. et al. Large-area synthesis of high-quality and uniform monolayer WS_2 on reusable Au foils. *Nat. Commun*. **2015**, *6*, 8569.

[20] Sarma, P. V.; Patil, P. D.; Barman, P. K.; Kini, R. N.; Shaijumon, M. M. Controllable growth of few-layer spiral WS_2. *RSC Adv*. **2016**, *6*, 376–382.

[21] Chen, K.; Wan, X.; Xie, W. G.; Wen, J. X.; Kang, Z. W.; Zeng, X. L.; Chen, H. J.; Xu, J. B. Lateral built-in potential of monolayer MoS_2-WS_2 in-plane heterostructures by a shortcut growth strategy. *Adv. Mater*. **2015**, *27*, 6431–6437.

[22] Xu, W. S.; Kozawa, D. C.; Zhou, Y. Q.; Wang, Y. Z.; Sheng, Y. W.; Jiang, T.; Strano, M. S.; Warner, J. H. Controlling photoluminescence enhancement and energy transfer in WS_2:hBN:WS_2 vertical stacks by precise interlayer distances. *Small* **2020**, *16*, 1905985.

[23] Park, J.; Kim, M. S.; Cha, E.; Kim, J.; Choi, W. Synthesis of uniform single layer WS_2 for tunable photoluminescence. *Sci. Rep*. **2017**, *7*, 16121.

[24] Hsu, W. T.; Quan, J. M.; Wang, C. Y.; Lu, L. S.; Campbell, M.; Chang, W. H.; Li, L. J.; Li, X. Q.; Shih, C. K. Dielectric impact on exciton binding energy and quasiparticle bandgap in monolayer WS_2 and WSe_2. *2D Mater*. **2019**, *6*, 025028.

[25] Chernikov, A.; Ruppert, C.; Hill, H. M.; Rigosi, A. F.; Heinz, T. F. Population inversion and giant bandgap renormalization in atomically thin WS_2 layers. *Nat. Photonics* **2015**, *9*, 466–469.

[26] Yue, Y. C.; Chen, J. C.; Zhang, Y.; Ding, S. S.; Zhao, F. L.; Wang, Y.; Zhang, D. H.; Li, R. J.; Dong, H. L.; Hu, W. P. et al. Two-dimensional high-quality monolayered triangular WS_2 flakes for field-effect transistors. *ACS Appl. Mater. Interfaces* **2018**, *10*, 22435–22444.

[27] Gong, Y. J.; Lin, Z.; Ye, G. L.; Shi, G.; Feng, S. M.; Lei, Y.; Elias, A. L.; Perea-Lopez, N.; Vajtai, R.; Terrones, H. et al. Tellurium-assisted low-temperature synthesis of MoS_2 and WS_2 monolayers. *ACS Nano* **2015**, *9*, 11658–11666.

[28] Liu, L. N.; Wu, J. X.; Wu, L. Y.; Ye, M.; Liu, X. Z.; Wang, Q.; Hou, S. Y.; Lu, P. F.; Sun, L. F.; Zheng, J. Y. et al. Phase-selective synthesis of 1T' MoS_2 monolayers and heterophase bilayers. *Nat. Mater*. **2018**, *17*, 1108–1114.

[29] Chen, J.; Jung, G. S.; Ryu, G. H.; Chang, R. J.; Zhou, S.; Wen, Y.; Buehler, M. J.; Warner, J. H. Atomically sharp dual grain boundaries in 2D WS_2 bilayers. *Small* **2019**, *15*, 1902590.

[30] Liu, C.; Xu, X. Z.; Qiu, L.; Wu, M. H.; Qiao, R. X.; Wang, L.; Wang, J. H.; Niu, J. J.; Liang, J.; Zhou, X. et al. Kinetic modulation of graphene growth by fluorine through spatially confined decomposition of metal fluorides. *Nat. Chem*. **2019**, *11*, 730–736.

[31] Sheng, Y. W.; Tan, H. J.; Wang, X. C.; Warner, J. H. Hydrogen addition for centimeter-sized monolayer tungsten disulfide continuous films by ambient pressure chemical vapor deposition. *Chem. Mater*. **2017**, *29*, 4904–4911.

[32] Wang, Y.; Kim, J. C.; Wu, R. J.; Martinez, J.; Song, X. J.; Yang, J.; Zhao, F.; Mkhoyan, A.; Jeong, H. Y.; Chhowalla, M. Van der Waals contacts between three-dimensional metals and two-dimensional semiconductors. *Nature* **2019**, *568*, 70–74.

[33] Khalil, H. M. W.; Khan, M. F.; Eom, J.; Noh, H. Highly stable and tunable chemical doping of multilayer WS_2 field effect transistor: Reduction in contact resistance. *ACS Appl. Mater. Interfaces* **2015**, *7*, 23589–23596.

[34] Iqbal, M. W.; Iqbal, M. Z.; Khan, M. F.; Kamran, M. A.; Majid, A.; Alharbi, T.; Eom, J. Tailoring the electrical and photo-electrical properties of a WS_2 field effect transistor by selective n-type chemical doping. *RSC Adv*. **2016**, *6*, 24675–24682.